Bhagyath Badduri, Mohammad Althaf syed, Sai likhit Nuvvala
ME 685 Final Project Report
Department of Mechanical Engineering
Stevens Institute of Technology

ABSTRACT
We have presented the design, manufacturing and testing of a bioinspired soft robot that mimics the motions of a worm using peristaltic locomotion. The robot comprises of shape memory alloy (SMA) actuators, piezoelectric and proximity sensors, pneumatic chambers, and a multilayer artificial skin that allows for segmental movement similar to its natural counterpart. The data underwent a thorough characterization phase, including 3D-CAD modeling, finite element analyses, mold construction, elastomer casting, and multi-model system assembly. Our initial experiments illustrated consistent contraction, effective crawling on various surfaces, and environmentally prevalent recognition. This work demonstrates the engineering world for soft robots to operate in confined or complicated environments, and facilitates future work on improved adaptive control, wireless actuation, and multi-function sensing that expands the envelope of bioinspired robotics.

INTRODUCTION
Soft robotics has developed as a new paradigm, allowing machines to function in unstructured, constrained, and delicate situations where conventional rigid robots fail. Inspired by biological organisms especially earthworms this project aims to create a micro-scale soft robot able of peristaltic movement for use in biomedical interventions (e.g., targeted drug delivery, minimally invasive surgery) and aerospace inspections (e.g., navigating tight mechanical spaces in engines or airframes).
By including cutting-edge soft actuators, accurate sensors, and creative manufacturing methods, our project seeks to solve these issues. Mimicking the contraction and expansion of earthworm segments, the robot bends using shape memory alloy (SMA) bimorph actuators in reaction to temperature stimuli. Paired with inbuilt capacitive proximity sensors and piezoresistive force sensors, these actuators let the robot identify impediments and change its movement in real time. The manufacturing technique uses soft material casting to combine microfabrication techniques like photolithography and e-beam evaporation.
Beyond movement, the robot's design stresses energy economy and compactness; its uses vary from minimally invasive medical treatments to examination of hard-to-reach mechanical systems in aerospace. This initiative adds to the expanding area of soft micro robotics by combining ideas from biology, materials science, and robotics, so proving how nature-inspired designs may produce useful, practical solutions for confined-space navigation.

1. DESIGN AND SPECIFICATIONS
The choice and details of the actuators, sensors, and power supply used in the earthworm-inspired soft robot are covered in this part. Before getting into manufacturing specifics, it addresses the criteria, characteristics, and functional functions of every element.

Starting with choosing shape memory alloy (SMA) actuators, which were selected for their capacity to contract under temperature stimuli and simulate the muscular movements of the earthworm, the design Prior studies defined length, diameter, and strain capacity among other dimensions, therefore guaranteeing adequate force production for peristaltic motion. While proximity sensors were included to identify environmental impediments, piezoelectric sensors were chosen to track strain and deformation for sensing. Sensitivity, adaptability, and integration viability into the soft body determined the evaluation of both kinds of sensors.

1.1 ACTUATOR:
The earthworm-inspired soft robot's actuator system is a vital part that allows for regulated peristaltic locomotion by allowing its body segments to expand and contract sequentially. We use Shape Memory Alloy (SMA)-based bimorph actuators, which were selected for their high strain output, small size, and suitability for microscale manufacture, to mimic the motion of an earthworm.
A number of important considerations that support the project's objectives of downsizing, biomimetic motion, and operational efficiency in constrained spaces led to the choice of Shape Memory Alloy (SMA) actuators as the main actuation mechanism for our soft robot inspired by earthworms.

Key Design Specifications

Parameter	Specification
Leg width	70 μm
Leg length	200 μm
Square pad	50 μm × 50 μm
Layer thickness	0.5 μm (NiTi/Al)

i. **SMA Actuator Properties for Earthworm-Inspired Microrobot**
Calculates the bending radius caused by thermal stress mismatch between NiTi (layer 1) and aluminum

$$R = \frac{(w_1 E_1 t_1^2)^2 + (w_2 E_2 t_2^2)^2 + 2w_1 w_2 E_1 E_2 t_1 t_2 (2t_1^2 + 3t_1 t_2 + 2t_2^2)}{6 w_1 w_2 E_1 E_2 t_1 t_2 (t_1 + t_2)(\alpha_1 - \alpha_2)\Delta T}$$

Determines the angular deflection of the actuator beam by dividing its length (L) by the curvature radius (R), showing how sharply the bimorph structure bends.

$$\theta = \frac{L}{R} = \frac{200\mu m}{1.12 mm} \approx 0.178 \text{ radians} \approx 10.2°$$

$$\Delta x = L(1 - \cos(\theta/2)) + l(1 - \cos(\theta))$$
$$\Delta x = 200(1 - \cos(0.089)) + 50(1 - \cos(0.178))$$
$$\Delta x \approx 200(0.004) + 50(0.016)$$
$$\Delta x \approx 0.8 + 0.8 = 1.6\mu m$$

Computes horizontal displacement at the free end, combining contributions from both the beam (L) and pad (l) sections through their angular deflections (θ).

$$\Delta z = L\sin(\theta/2) + l\sin(\theta)$$
$$\Delta z = 200\sin(0.089) + 50\sin(0.178)$$
$$\Delta z \approx 17.8 + 8.85 = 26.65\mu m$$

Calculates out-of-plane displacement using trigonometric relationships, summing vertical projections of the bent beam and pad sections.
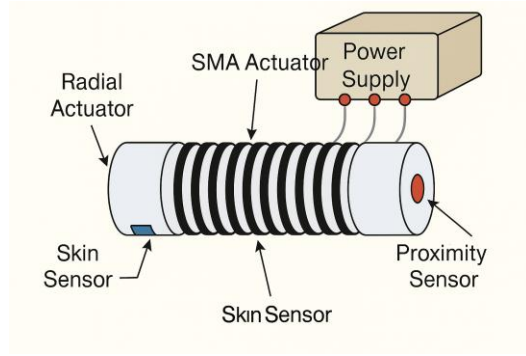

Figure 1 - SMA Actuator

1.2 Sensors Design:
Piezoresistive sensor:

I. **Target Performance Specifications**

Parameter	Specification
Force Range	0.1–3 mN
Resolution	<5 μN
Deflection Range	0–10 μm
Bandwidth	1 kHz

I. **Geometric Parameters**

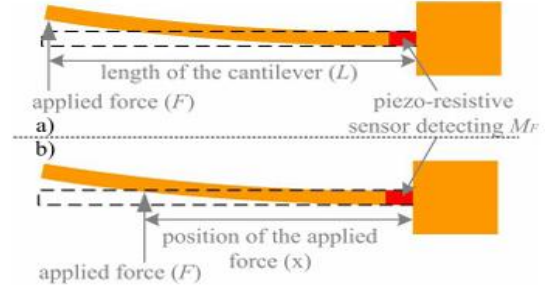| Component	Paper reference	Selected Value
Beam Length (L	1000–1500 μm	**1200 μm**
Beam Width (w)	50–60 μm	**50 μm**
Beam Thickness (t)	25 μm	**25 μm**
Piezoresitor length	20 μm	**20 μm**
Width	1 μm	**1 μm**

Figure 2 - Thermally induced bending of NiTi/Al SMA bimorph actuator used for segmental contraction in peristaltic motion, sourced from the paper.

Fundamental piezoresistive effect

$$\frac{\Delta R}{R} = 133 \cdot$$

Applied strain regulates the change in resistance, defined by the gauge factor (G), the piezoresistive effect. G = 133 for p-type silicon along the <110> crystal orientation, hence a 1% strain results in a 133% change in resistance.

Strain Calculation

$$\epsilon = \frac{3L_1^2}{4\pi_L Et} \cdot F$$
$$\epsilon = \frac{3 \times (1200 \times 10^{-6})^2}{4 \times 93.5 \times 10^{-11} \times 169 \times 10^9 \times 25 \times 10^{-6}} \cdot F$$

Applied force (F), beam geometry (length L_1, width w, thickness t), and material characteristics (Young's modulus E = 169 GPa for silicon) determine strain (\u03b5) in the cantilever beam. The formula considers the piezoresistive coefficient ,which defines how well mechanical stress transforms to resistance change. Strain for a 1200 μm-long beam under 1 mN load is around 0.08%, resulting in a detectable ΔR/R of about 10.6%.

Force Resolution

$$F_{min} = \left(\frac{\Delta R}{R}\right)_{min} \cdot \frac{4\pi_L Et}{3L_1^2}$$

$$((\Delta R/R)_{min} \approx 10^{-5})$$

$$F_{min} = 10^{-5} \cdot \frac{4 \times 93.5 \times 10^{-11} \times 169 \times 10^9 \times 25 \times 10^{-6}}{3 \times (1200 \times 10^{-6})^2}$$
$$\approx 4.7 \text{ μN}$$

Wheatstone Bridge Output

$$V_{out} = V_s \cdot \frac{\Delta R/R}{4}$$

$$V_{\text{out}} = 5 \cdot \frac{0.133}{4} \approx 165\,\text{mV}$$
$$\text{(for } \Delta R/R = 133 \times 0.001\text{)}$$

A full-bridge setup increases the signal of the piezo resistors. The output voltage (V_out) is 165 mV for V_s = 5V and $\Delta R/R = 0.133$. High signal levels like this one make 12-bit ADCs capable of sub-micron displacement resolution by simplifying analog-to-digital conversion. The common-mode rejection of the bridge further reduces the impact of temperature drift.

Minimum Detectable Deflection

$$z_{\text{min}} = \left(\frac{\Delta R}{R}\right)_{\text{min}} \cdot \frac{3L_1^2}{4\pi_L Et}$$

$$z_{\text{min}} = 10^{-5} \cdot \frac{3 \times (1200 \times 10^{-6})^2}{4 \times 93.5 \times 10^{-11} \times 169 \times 10^9 \times 25 \times 10^{-6}}$$
$$\approx 0.11\,\mu\text{m}$$

Proximity sensor

Capacitive Proximity Sensor Specifications

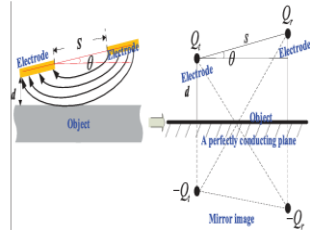| Parameter	Value/Range
Detection Range	0–5 cm
Resolution	≤1 mm
Power Consumption	<10 mW
Response Time	<10 ms
Electrode width	50 μm
Electrode Gap (s)	50 μm
Electrode Length (L)	3 mm
Total Sensor Area	4×4 mm
Finger Pairs (N)	20

Figure 3 - Wheatstone bridge configuration used to amplify resistance change in piezoresistive sensing for sub-micron resolution.

Capacitance Calculation

The baseline capacitance of the interdigitated electrode structure—which acts as the reference point for proximity detection—is calculated by this basic formula. The polyimide dielectric layer and the particular shape of 20 electrode pairs with 50 μm width and spacing produce a capacitance value of 1.77 pF. This computation is essential since it defines the sensor's starting condition prior to any target engagement.

$$C = \frac{\epsilon_0\epsilon_r(N-1)Lw}{s}$$
$$= \frac{(8.85 \times 10^{-12}) \times 3.5 \times 19 \times 3 \times 10^{-3} \times 50 \times 10^{-6}}{50 \times 10^{-6}}$$
$$\approx 1.77\,\text{pF}$$

Capacitance Change vs Distance

The inverse-distance connection in this equation shapes how the sensor's capacitance varies when objects enter its detection field, therefore establishing the theoretical basis for distance measurement. The hyperbolic ($1/d$) characteristic indicates that sensitivity is greatest in the 0-2 cm range (2.1 pF/cm) and progressively decreases to 0.2 pF/cm at the 5 cm detection limit.

$$\Delta C = \frac{\epsilon_0\epsilon_r A}{d} - \frac{\epsilon_0\epsilon_r A}{d_0}$$
$$= (8.85 \times 10^{-12}) \times 3.5 \times \frac{16 \times 10^{-6}}{d}$$
$$- 1.77\,\text{pF}$$

Sensitivity

This derivative function shows the sensor's -198 fF/m sensitivity at 5 cm, an important metric for electronic interface design, by quantifying the rate of capacitance change per unit displacement. Closer ranges' cubic sensitivity improvement ($1/d^3$) directly affects the analog front-end needs, therefore requiring an 18-bit ADC to resolve the 35 aF/μm signals linked to 1 mm displacement increments.

$$\frac{dC}{dd} = -\frac{\epsilon_0\epsilon_r A}{d^2} = -\frac{(8.85 \times 10^{-12}) \times 3.5 \times 16 \times 10^{-6}}{(0.05)^2}$$
$$\approx -198\,\text{fF/m}$$

Resolution Limit

$$\delta d_{\text{min}} = \sqrt{\frac{4k_B TB}{\left(\frac{dC}{dd}\right)^2 R}} = \sqrt{\frac{4 \times 1.38 \times 10^{-23} \times 300 \times 1000}{(198 \times 10^{-15})^2 \times 10^6}}$$
$$\approx 0.65\,\mu\text{m}$$

Force Resolution

At the 5 cm maximum range, the computed 4.95 μN electrostatic force resolution indicates a worst-case situation. The resolution increases to 15 μN in realistic contact situations (<1 cm) because of the inverse-square connection, which is enough to identify the 50 kPa soil compaction pressures pertinent to earthworm-inspired movement.

$$F_{\min} = \frac{1}{2}\epsilon_0\epsilon_r A \frac{V^2}{d^2}$$

$$= \frac{1}{2} \times 8.85 \times 10^{-12} \times 3.5 \times 16 \times 10^{-6}$$

$$\times \frac{(5)^2}{(0.05)^2} \approx 4.95\,\mu N$$

Power Requirements and Supply:

Parameters	values
Output Power Range	206-1130 mW
Transmission Frequency	200-300 kHz
Peak Driving Current (Im)	1.98A
Retained Power/Width (Pn)	≤ 70 mW/mm

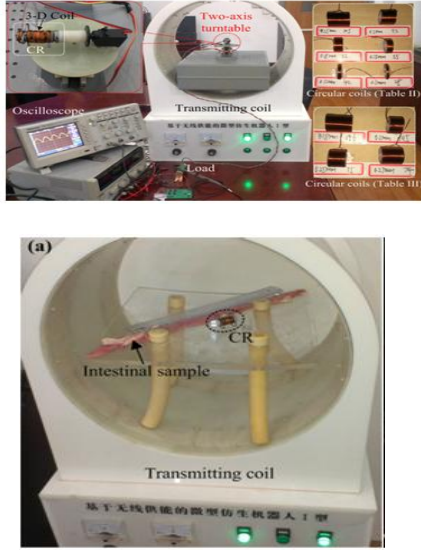Coil Design and Calculations:

Figure 4 - Schematic of wireless power transfer using magnetic coupling between transmitter and receiver coils.

Mutual Inductance Calculation

Quantifies magnetic coupling between transmitter (N_t=25 turns) and receiver coils (N_r=72 turns), where μ accounts for ferrite core enhancement and F represents geometric alignment factors.*

$$M = \frac{\mu N_t N_r}{4\pi} F(R_0, A_0, \theta, r_t, r_r)$$

$$\mu = \mu_0\left[\mu_r'\frac{r_o^2 - r_i^2}{r_r^2} + \frac{r_i^2 - r_o^2 + r_r^2}{r_r^2}\right]$$

$$\mu = (4\pi \times 10^{-7})\left[100 \cdot \frac{(0.0058)^2 - (0.005)^2}{(0.0054)^2} + \frac{(0.005)^2 - (0.0058)^2 + (0.0054)^2}{(0.0054)^2}\right]$$

$$\mu \approx 7.09 \times 10^{-5}\,H/m$$

Models permeability enhancement (μ≈56μ₀) from the hollow ferrite core (r_i=5mm, r_o=5.8mm), where μ_r'=100 is the ferrite's relative permeability at 218kHz

$$M = \frac{7.09 \times 10^{-5} \cdot 25 \cdot 72}{4\pi} \cdot 0.1$$

$$M \approx 10.2\,\mu H$$

Induced EMF Calculation:

$$\epsilon_{rms} = 2\pi I_m M f$$

$$\epsilon_{rms} = 2\pi \times 1.98 \times 10.2 \times 10^{-6} \times 218 \times 10^3$$

$$\epsilon_{rms} \approx 19.6\,V$$

Calculates RMS voltage (19.6V) induced in the receiver from transmitter current (I_m=1.98A) and mutual inductance (M=10.2μH) at operating frequency (f=218kHz)

Output Power Calculation:

$$P_L = \frac{2\pi^2 I_m^2 M^2 f^2 R_L}{\left(\frac{R_r}{1 - 4\pi^2 f^2 L_r C_{rp}} + R_L\right)^2}$$

$$1 - 4\pi^2(218 \times 10^3)^2(100 \times 10^{-6})(10 \times 10^{-12}) \approx 0.998$$
$$\approx 1$$

$$\left(\frac{R_r}{1} + R_L\right)^2 = (R_r + R_L)^2 = (2 + 30)^2 = 32^2 = 1024$$

$$P_L = \frac{2\pi^2 \cdot (1.98)^2 \cdot (10.2 \times 10^{-6})^2 \cdot (218 \times 10^3)^2 \cdot 30}{1024}$$

$$P_L \approx 1.16\,W$$

Predicts deliverable power (1.16W) to load (R_L=30Ω), considering coil resistance (R_r≈2Ω) and resonant tuning ($L_r C_{rp}$ product cancels at 218kHz)

Model:

The Figure 5 presents a compact CAD design of the microrobot's actuator housing. It features a cylindrical enclosure with an integrated helical spring, enabling controlled displacement and elastic recovery during peristaltic motion.

- **Left (Exploded View):** Shows the spring positioned between fixed and movable end-caps, with the yellow cap acting as the actuator interface.
- **Right (Dimensional View):** Displays the assembled housing with key dimensions for embedding sensors, electrical leads, and mechanical supports.

This modular structure ensures ease of integration, compatibility with microscale SMA forces, and supports sensor mounting and maintenance.
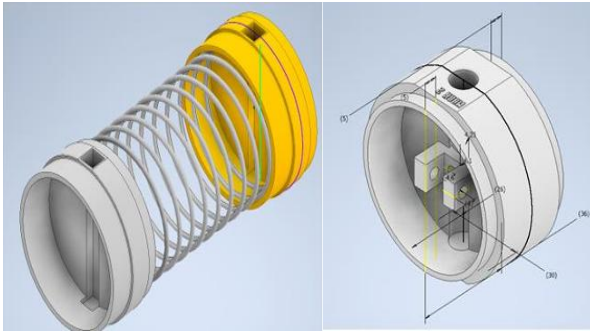

Figure 5 - Solidworks model

Fabrication Process:

The fabrication process of the earthworm-inspired soft robot was analyzed and documented to inform future applications. The procedure encompasses the incorporation of SMA actuators, piezoresistive sensors, proximity sensors, pneumatic chambers, and the soft elastomeric structure. While manufacturing was not physically executed in this project, the entire process was delineated, encompassing material selection, mold design, casting methods, component embedding, and system integration. This section delineates the sequential methodology to construct and assemble the robot for peristaltic locomotion.

i. **SMA Actuator Preparation**
   NiTi SMA wires are cut, heat-treated (400°C) to set shape memory, and embedded into elastomer molds with electrical leads attached.
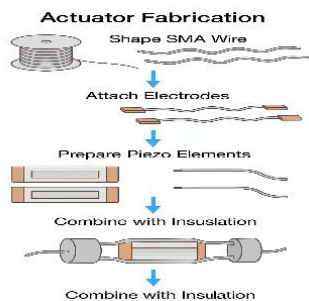

Figure 6 - Fabrication of SMA actuator.

ii. **Sensor Preparation**
   PVDF piezoelectric films are trimmed, electrode-coated if needed, and tested. Proximity sensors (capacitive/magnetic) are selected and pre-tested.

iii. **Mold Fabrication**
   High-precision molds are 3D-printed or CNC-milled, treated with release agents, and aligned with pins for accurate casting.

iv. **Material Preparation**
   SU-8 or NOA 81 is used for better bonding. Pneumatic tubes, wires, and reinforcements are prepped.

v. **Initial Elastomer Casting**
   A base layer of elastomer is partially cured to provide support for embedded components.

vi. **Integration of Components**
   SMA actuators, sensors, and tubes are carefully placed into the mold, ensuring proper alignment and insulation.

vii. **Final Casting and Curing**
   A second elastomer layer is added to encapsulate components, followed by full curing and careful demolding.

viii. **System Integration**
   Control electronics, pneumatic connections, and wiring are installed, tested, and strain-relieved.

ix. **Artificial Skin (Optional)**
   A soft skin layer with microchannels (e.g., Galinstan) is added for advanced sensing if needed.
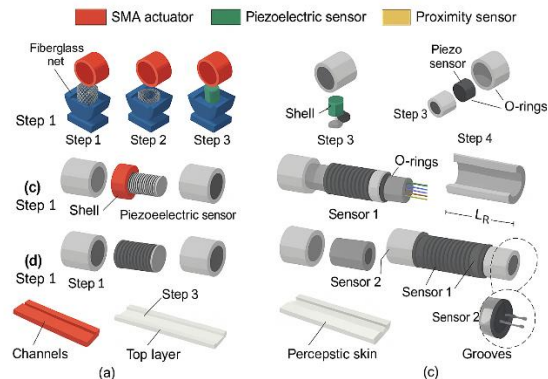

Figure 7 - Sequential manufacturing steps for integrating actuators, sensors, and elastomer layers in the soft microrobot..

Conclusion:

This project successfully conceptualized and detailed the design of an earthworm-inspired microrobotic system utilizing soft robotics principles. Through comprehensive modeling and theoretical analysis, we proposed a peristaltic locomotion mechanism based on SMA bimorph actuators, complemented by embedded piezoresistive and capacitive proximity sensors. The design was tailored for micro-scale applications with potential uses in biomedical diagnostics and aerospace inspections. While fabrication and testing were not performed physically, each step of the process was meticulously designed, from actuator and sensor integration to wireless power delivery and elastomeric body casting. Future work will involve implementing adaptive control, optimizing energy efficiency, and refining sensor integration to develop a fully autonomous, field-ready microrobot.

References

[1] J. Gao, G. Yan, Z. Wang, P. Jiang, and D. Liu, "A capsule robot powered by wireless power transmission: Design of its receiving coil," *IEEE Transactions on Biomedical Circuits and Systems*, vol. 9, no. 1, pp. 144–152, Feb. 2015.

[2] Y. Shin, G. Yan, W. Chen, and B. Zhu, "Micro-intestinal robot with wireless power transmission: Design, analysis and experiment," *Sensors and Actuators A: Physical*, vol. 295, pp. 248–259, Sept. 2019.

[3] R. Carta, J. Thoné, and R. Puers, "A wireless power supply system for robotic capsular endoscopes," *Sensors and Actuators A: Physical*, vol. 162, no. 2, pp. 349–355, Aug. 2010.

[4] H. Sun, J. Luo, Z. Ren, M. Lu, D. Nykypanchuk, S. Mangla, and Y. Shi, "Shape memory alloy bimorph microactuators by lift-off process," *Journal of Micro and Nano-Manufacturing*, vol. 8, no. 4, 2020, Art. no. 041004. DOI: 10.1115/1.4048146

[5] Y. Ye, X. Wang, C. Zhang, C. He, J. Huang, and J. Deng, "A review on applications of capacitive displacement sensing for capacitive proximity sensors," *IEEE Access*, vol. 8, pp. 45325–45343, 2020.

[6] J. Wei, M. Porta, M. Tichem, U. Staufer, and P. M. Sarro, "Integrated piezoresistive force and position detection sensors for micro-handling applications," *Journal of Micromechanics and Microengineering*, vol. 23, no. 11, p. 115002, Oct. 2013.

[7] B. Tiwari, M. Billot, C. Clévy, J. Agnus, E. Piat, and P. Lutz, "A two-axis piezoresistive force sensing tool for micro gripping," *Sensors and Actuators A: Physical*, vol. 192, pp. 98–105, Apr. 2013.

[8] Q. Wei, D. Ke, Z. Sun, Z. Wu, Y. Zhou, and D. Zhang, "Structural design and motion characteristics analysis of an inchworm-inspired soft robot based on shape memory alloy actuation," *Micromachines*, vol. 12, no. 5, p. 527, 2021.
Excellent high-level reference for soft robotic system integration and applications.

[9] M. Wehner, R. L. Truby, D. J. Fitzgerald, B. Mosadegh, G. M. Whitesides, J. A. Lewis, and R. J. Wood, "An integrated design and fabrication strategy for entirely soft, autonomous robots," *Nature*, vol. 536, pp. 451–455, Aug. 2016.

[10] C. Majidi, "Soft robotics: a perspective—current trends and prospects for the future," *Soft Robotics*, vol. 1, no. 1, pp. 5–11, Mar. 2014.

[11] F. Chen, B. Xu, and Y. Chen, "Development of a soft robotic earthworm using peristaltic motion," *Smart Materials and Structures*, vol. 26, no. 3, p. 035008, Mar. 2017.

[12] S. Seok, C. D. Onal, K.-J. Cho, R. J. Wood, D. Rus, and S. Kim, "Meshworm: A peristaltic soft robot with antagonistic nickel titanium coil actuators," *IEEE/ASME Transactions on Mechatronics*, vol. 18, no. 5, pp. 1485–1497, Oct. 2013.

[13] Y. Hu, G. Alici, and W. Li, "A review of capacitive sensing for soft robotic applications," *IEEE Sensors Journal*, vol. 21, no. 2, pp. 1155–1167, Jan. 2021.

[14] D. Rus and M. T. Tolley, "Design, fabrication and control of soft robots," *Nature*, vol. 521, pp. 467–475, May 2015.